A Finite-Volume Formulation for Fully Compressible Premixed Combustion using the Level Set Approach

D. HARTMANN, M. MEINKE, W. SCHRÖDER

Institute of Aerodynamics (AIA), RWTH Aachen University, Wüllnerstr. 5a, 52062 Aachen, Germany

Abstract :

The level set approach is used for fully compressible simulations of premixed combustion. The motivation of the present work is to numerically simulate thermo-acoustic combustion instabilities. These instabilities are excited by the interaction of heat release and pressure fluctuations, which can numerically only be accurately accounted for in fully compressible simulations. A major challenge is the discretization and the inclusion of the heat release due to combustion at the flame front. To this end, a finite-volume formulation, which uses the ideas of the ghost-fluid method [Fedkiw et al. J. Comp. Phys. 154, 393-427 (1999)], is developed based on a low-dissipation scheme which has been successfully used for large-eddy simulations of non-reacting flows.

Mots clefs : Level set approach, G-equation, Premixed combustion, Compressible Navier-Stokes equations

1 Introduction

The numerical simulation of thermoacoustic instabilities in premixed combustion resolving the (turbulent) flow, the chemical reactions, and the acoustic field is a very challenging task due to the disparity of length scales involved. Premixed combustion often occurs in thin layers, in which diffusive transport and chemical reactions are strongly coupled. A common modeling approach in the numerical simulation of turbulent premixed combustion is the flamelet assumption, which states that the length scale of the combustion process is smaller than the smallest scale of the turbulent flow. Hence, to simulate the turbulent reacting flow field, the premixed flame can be viewed as an infinitely thin interface, which is commonly referred to as the flame front. The idea of tracking a propagating interface to describe the motion of the premixed flame front was introduced by Markstein [1], which later led to the formulation of the G-equation [2].
The G-equation describes only the motion of the flame front in the flow field, which is in the present context compressible including acoustic waves, and does not incorporate the local heat release of the premixed flame. At the discontinuous flame front jumps in the density and the normal velocity due to the thermal expansion are encountered. At small Mach numbers the pressure jump is relatively small and is often neglected. The discontinuous density and velocity profile make the discretization at the flame front difficult. Additionally, the heat release due to combustion at the flame front must be accounted for.
The objective of this contribution is to present a finite-volume scheme for fully compressible large-eddy simulation of premixed combustion using the G-equation approach. The baseline numerical scheme to discretize the compressible Navier-Stokes equations involves the advection upstream splitting method (AUSM) [3] with a low-dissipation pressure splitting to compute the convective flux and has been successfully used in large-eddy simulations of non-reacting flows [4]. This scheme is extended to be capable of accounting for a premixed flame front the motion of which is governed by the G-equation. The necessary modifications are formulated drawing on the ideas of the ghost fluid method [5].

2 Mathematical model

Let the density be denoted by ϱ, the Cartesian components of the velocity vector $\mathbf{v}$ in the x_i directions of $\mathbf{x}$ be given by v_i ($i = \{0, 1, 2\}$), and the total specific energy and the pressure be represented by $E = e + \frac{\mathbf{v}^2}{2}$ and p, respectively. The quantity e denotes the specific internal energy and t denotes the time. We consider the compressible Navier-Stokes equations in their non-dimensional form, which can be written as

$$\partial_t \mathbf{Q} + \boldsymbol{\nabla} \overline{\mathbf{H}} = \mathbf{0}, \tag{1}$$

with $\mathbf{Q} = [\varrho, \varrho\mathbf{v}, \varrho E]^T$ being the vector of the conservative variables and $\overline{\overline{\mathbf{H}}} = [\mathbf{F}_0, \mathbf{F}_1, \mathbf{F}_2]^T$ being the flux vector containing an inviscid part $\overline{\overline{\mathbf{H}}}^i$ and a viscous part $\overline{\overline{\mathbf{H}}}^v$

$$\overline{\overline{\mathbf{H}}} = \overline{\overline{\mathbf{H}}}^i - \overline{\overline{\mathbf{H}}}^v = \begin{pmatrix} \varrho\mathbf{v} \\ \varrho\mathbf{v}\mathbf{v} + p \\ \mathbf{v}(\varrho E + p) \end{pmatrix} + \frac{1}{Re} \begin{pmatrix} 0 \\ \overline{\boldsymbol{\tau}} \\ \overline{\boldsymbol{\tau}}\mathbf{v} + \mathbf{q} \end{pmatrix}, \tag{2}$$

where $\mathbf{q}$ contains the heat conduction terms. The superscript T identifies the vector transpose and $\boldsymbol{\nabla}$ denotes the vector of spatial derivatives in the Cartesian coordinate system, $\boldsymbol{\nabla} = [\partial_{x_0}, \partial_{x_1}, \partial_{x_2}]^T$. Furthermore, let $\mathbf{P}$ designate the vector of primitive variables, $\mathbf{P} = [\varrho, \mathbf{v}, p]^T$. The Reynolds number is given by $Re = \frac{\varrho_\infty v_\infty l}{\mu_\infty}$, where l is a characteristic length. The dynamic viscosity μ is computed using a Sutherland law. We assume a Newtonian fluid such that the components τ_{ij} of the second-rank stress tensor $\overline{\boldsymbol{\tau}}$ can be formulated by

$$\tau_{ij} = -2\mu S_{ij} + \frac{2}{3}\mu S_{ij}\delta_{ij}, \tag{3}$$

where the S_{ij} are the components of the rate-of-strain tensor

$$\overline{\mathbf{S}} = \frac{1}{2}\left(\boldsymbol{\nabla}\mathbf{v} + (\boldsymbol{\nabla}\mathbf{v})^T\right). \tag{4}$$

The vector of heat conduction $\mathbf{q}$ is accounted for by Fourier's law

$$\mathbf{q} = -\frac{k}{Pr(\gamma - 1)}\boldsymbol{\nabla}T, \tag{5}$$

where γ is the ratio of specific heats. The Prandtl number $Pr = \frac{\mu_\infty c_p}{k_\infty}$ contains the specific heat at constant pressure c_p. Finally, the thermal conductivity is evaluated from $k(T) = \mu(T)$, which holds for a constant Prandtl number.
Using the Gauss divergence theorem, the integral form of the Navier-Stokes equations suitable for a finite-volume discretization is obtained as

$$\int_V \partial_t \mathbf{Q} dV + \int_A \overline{\overline{\mathbf{H}}}\,\mathbf{n} dA = \mathbf{0}, \tag{6}$$

where $\mathbf{n}$ is the outward unit normal vector on the surface dA.

2.1 G-equation to describe the flame front motion

As a gasdynamic discontinuity, the flame front is in the level set approach represented by a hypersurface associated with the contour $G_0 = \{(\mathbf{x}, t) : G(\mathbf{x}, t) = 0\}$ of the scalar field G. The interface G_0 is in this approach implicitly captured rather than explicitly tracked. The evolution of the scalar G carrying the information on the location of the flame front is governed by the G-equation, which is written

$$\frac{\partial G}{\partial t} + \mathbf{f} \cdot \boldsymbol{\nabla} G = 0, \tag{7}$$

where $\mathbf{f} = \mathbf{v} + (s_l^u + s_\kappa^u)\mathbf{n}$ is the local extension velocity of the flame front with the outward normal vector $\mathbf{n}$. Here, s_l^u denotes the laminar burning velocity with respect to the unburnt gas, and s_κ^u is the flame front motion due to its curvature κ, which can be computed directly from the scalar G field by

$$\kappa = \boldsymbol{\nabla} \cdot \mathbf{n}, \qquad \mathbf{n} = -\frac{\boldsymbol{\nabla} G}{|\boldsymbol{\nabla} G|}. \tag{8}$$

3 Numerical method

The level set solver and the flow solver are coupled in a hierarchical dual-mesh framework. Similar approaches have been presented in [6, 7]. In this dual-mesh framework, the G-equation and the compressible Navier-Stokes equations can be solved on different grids, such that a locally refined grid can be used for the flow solver, while the G-equation can be discretized with high-order spatial accuracy on a uniformly spaced grid. In the present context, Cartesian grids are used for both solvers, and the cells are organized in hierarchical cell-tree data structures sharing the same root cell, as illustrated in Fig. 1. This significantly simplifies the data transfer, which, in the present work, is only required on the cells directly at the front. Assuming there is a level r which both trees have in common and the flow grid is not finer than the G grid around the flame front, the data synchronization between the grids is performed in 4 steps :

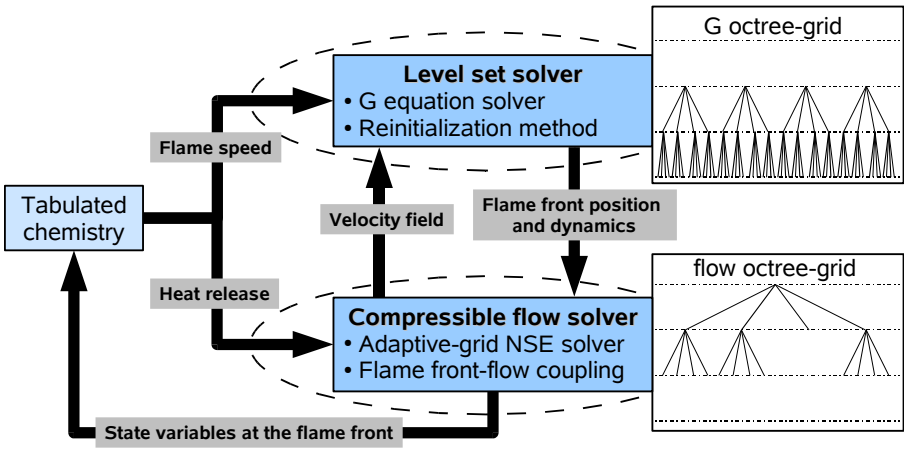

FIG. 1 – Coupling of the adaptive-grid flow solver and the level set solver in a dual-mesh framework, which is based on hierarchical Cartesian grids.

1. Average the G-field from cell levels $r+i,\ i>0$, to level r on the G grid.
2. Transfer G from the level set solver to the flow solver.
3. Transfer the flow velocity vector $\mathbf{v}$ from the flow solver to the level set solver.
4. Interpolate $\mathbf{v}$ from level r to higher grid levels on the G grid.

Since both solvers can access the data from all grids at all times, step 2 is not explicitly performed.

3.1 Level set transport

The G-equation (7) is integrated in time using a third-order 3-stage Runge-Kutta scheme and discretized in space using a fifth-order upstream-central finite-difference scheme. For efficiency, a fast, localized level set method is used, i.e., the G-field is evolved only in a narrow band around the flame front. For details we refer to [8]. It is common practice to initialize the G-field into a signed distance function with respect to the flame front, i.e., $|\boldsymbol{\nabla} G| = 1$, and it is well known [9, 8] that the G-field must be frequently reinitialized to approximately maintain this property. It has been shown that the reinitialization can be of crucial importance for the accuracy of the level set solution and that inappropriate or too infrequent reinitialization significantly degrades the solution accuracy [10]. In this work, the constrained reinitialization equation

$$\begin{cases} \dfrac{\partial G}{\partial \tau} + S(G(\tau=0))(|\boldsymbol{\nabla} G| - 1) = \beta F, \\ S(G) = \dfrac{G}{\sqrt{G^2 + h^2}}, \end{cases} \tag{9}$$

developed in [11] is solved in artificial time τ to reinitialize the level set function. The left-hand side of Eq. (9) is formulated to restore the property $|\boldsymbol{\nabla} G| = 1$, while the forcing term F weighted by $\beta = 0.5$ on the right-hand side corrects the displacement of the flame front, which occurs during the reinitialization. The formulation HOCR-2 [11], which is based on the constrained reinitialization scheme developed in [8], is used to formulate the forcing term. Like the G-equation (7), Eq. (9) is only solved in a narrow band around the flame front.
Since the flame speed is only defined at the flame front and the accuracy of the level set solution significantly benefits from a smooth distribution of the extension velocity $\mathbf{f}$ in the narrow band, the PDE-based method of [12] is used to provide the extension velocity $\mathbf{f}$ in the narrow band.

3.2 Discretization of the Navier-Stokes equations

The compressible Navier-Stokes equations are discretized using a finite-volume formulation on an adaptively refined Cartesian grid [13, 14]. Embedded boundaries are represented by means of cut-cells, such that the present method can be used to simulate flows in complex geometries such as gas turbines or engines.
A difficulty in representing the flame front by a gasdynamic discontinuity is the discretization of the governing equations at the front. Furthermore, the heat release due to combustion at the flame front must be taken into account, i.e., the unburnt and the burnt states ahead of and behind the front have to be coupled. The objective is to derive a consistent and low-dissipation flux formulation, which can be used for large-eddy simulations of premixed combustion.

3.2.1 Inviscid flux

For a clear description, we refer in the following to a uniformly spaced grid with a meshwidth h. Consider a surface between two cells L and R. First, the discretization of the convective terms is discussed. The convective flux at the surface is computed based on left and right interpolated variables using an appropriate scheme represented by the operator F,

$$F = F\left(\mathbf{P}^L, \mathbf{P}^R\right). \tag{10}$$

Consider now the case that the cells L and R are on different sides of the flame front. To achieve an oscillation-free discretization and to account for the heat release at the flame front, we consider two fluid states, the unburnt state and the burnt state, which are separately evolved. That is, to discretize the unburnt state no data of the burnt state is directly used and vice versa. In this case, two fluxes are computed on the surface

$$\left.\begin{aligned} F^u &= F\left(\mathbf{P}^{u,L}, \widetilde{\mathbf{P}^{u,R}}\right) \\ F^b &= F\left(\widetilde{\mathbf{P}^{b,L}}, \mathbf{P}^{b,R}\right) \end{aligned}\right\} \quad \text{if} \quad G^L < 0,\ G^R > 0, \tag{11}$$

$$\left.\begin{aligned} F^u &= F\left(\widetilde{\mathbf{P}^{u,L}}, \mathbf{P}^{u,R}\right) \\ F^b &= F\left(\mathbf{P}^{b,L}, \widetilde{\mathbf{P}^{b,R}}\right) \end{aligned}\right\} \quad \text{if} \quad G^L > 0,\ G^R < 0, \tag{12}$$

where the superscripts u and b denote the unburnt state and the burnt state, respectively. The vectors of ghost variables $\widetilde{\mathbf{P}^{u,R}}$ and $\widetilde{\mathbf{P}^{b,L}}$ in Eq. (11) and $\widetilde{\mathbf{P}^{u,L}}$ and $\widetilde{\mathbf{P}^{b,R}}$ in Eq. (12) cannot be reconstructed from the respective side of the flame front since the required fluid state is not available. However, the unburnt and the burnt interpolated variables on the surface must satisfy the Rankine-Hugoniot relations requiring the conservation of mass, momentum, and energy across the moving flame front, which can be written neglecting viscous and heat conduction fluxes

$$\left\langle \begin{array}{c} \mathfrak{F}_\varrho \\ \mathfrak{F}_{\varrho v_n} \\ \mathfrak{F}_{\varrho E} \end{array} \right\rangle = \mathbf{0}, \tag{13}$$

where $\langle \mathfrak{F} \rangle$ denotes the jump of $\mathfrak{F}$ across the flame front and the fluxes are evaluated in a frame of reference moving along with the flame front, that is,

$$\mathfrak{F}_\varrho = \varrho(v_n - f_n), \tag{14}$$

$$\mathfrak{F}_{\varrho v_n} = \varrho(v_n - f_n)^2 + p, \tag{15}$$

$$\mathfrak{F}_{\varrho E} = \left(\varrho e + \frac{\varrho(v_n - f_n)^2}{2} + p\right)(v_n - f_n). \tag{16}$$

The quantities $v_n = \mathbf{v} \cdot \mathbf{n}$ and $f_n = \mathbf{f} \cdot \mathbf{n}$ are the normal flow velocity and the normal extension velocity with respect to the flame front normal vector. The unknown ghost variables $\widetilde{\mathbf{P}^u}$ and $\widetilde{\mathbf{P}^b}$ can then be computed by solving the system

$$\left(\begin{array}{c} \widetilde{\mathfrak{F}_\varrho} \\ \widetilde{\mathfrak{F}_{\varrho v_n}} \\ \widetilde{\mathfrak{F}_{\varrho E}} \end{array} \right)^u = \left(\begin{array}{c} \mathfrak{F}_\varrho \\ \mathfrak{F}_{\varrho v_n} \\ \mathfrak{F}_{\varrho E} \end{array} \right)^b, \quad \left(\begin{array}{c} \widetilde{\mathfrak{F}_\varrho} \\ \widetilde{\mathfrak{F}_{\varrho v_n}} \\ \widetilde{\mathfrak{F}_{\varrho E}} \end{array} \right)^b = \left(\begin{array}{c} \mathfrak{F}_\varrho \\ \mathfrak{F}_{\varrho v_n} \\ \mathfrak{F}_{\varrho E} \end{array} \right)^u, \tag{17}$$

supplemented by the equation of state for the ghost variables

$$\tilde{p} = (\tilde{\gamma} - 1)\,\tilde{\varrho}\tilde{e}, \tag{18}$$

which is evaluated in the unburnt and in the burnt gas, respectively. The system of equations (17) can be manipulated using Eq. (18) to obtain algebraic expressions for the ghost variables $\widetilde{\mathbf{P}}$, which have been used to formulate the ghost fluid method in [5].

What remains is to determine the left and right interpolated variables on the surface and the flux function F. We use the advection upstream splitting scheme [3] to compute the convective flux with a modified low-dissipation pressure splitting scheme as proposed in [4] in the context of large-eddy simulation of non-reacting flows. As in [4], the interpolated primitive variables are obtained using the MUSCL approach [15]. Second-order accuracy is obtained by computing the cell center gradients using a central-difference scheme. On the cells at the flame front, the stencil of this scheme includes one cell at a different state, see Fig. 2, and the principle of the ghost-fluid method is used as above by solving Eq. (17) to reconstruct the required ghost variables on the cell. That is, in the case illustrated in Fig. 2a, the unburnt variables $\mathbf{P}^u_{j-1}$ and $\widetilde{\mathbf{P}^u_{j+1}}$ are used to compute the derivative on j, and in the case illustrated in Fig. 2b, the burnt variables $\widetilde{\mathbf{P}^b_j}$ and $\mathbf{P}^b_{j+2}$ are used to

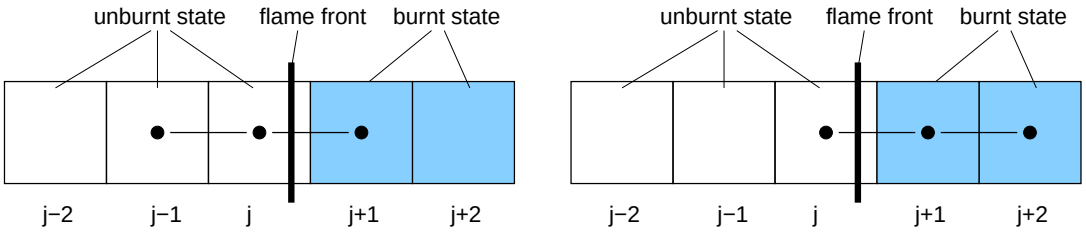

FIG. 2 – Illustration of the discretization at the flame front : (a) the stencil of the center difference on j, which is in the unburnt state, reaches over the flame front and includes $j+1$, which is in the burnt state ; (b) the stencil of the center difference on $j+1$, which is in the burnt state, reaches over the flame front and includes j, which is in the unburnt state.

compute the derivative on $j+1$. The ghost variables $\widetilde{\mathbf{P}_j^u}$ and $\widetilde{\mathbf{P}_{j-1}^b}$ are obtained from $\mathbf{P}_j^b$ and $\mathbf{P}_{j-1}^u$ by solving Eq. (17) as aforementioned.
Note, the cell-center ghost variables are needed only once to compute the cell center gradient. Furthermore, the surface ghost variables are needed only once to compute the ghost flux. Hence, all ghost variables can be computed at the time they are needed, such that the modifications of the standard finite-volume method do not cause any memory overhead. Finally, in the presented second-order accurate scheme, the ghost variables are only needed on the cells at the flame front and on the surfaces between cells of different state. Hence, the Rankine-Hugoniot relations need to be applied only very locally around the flame front.

3.2.2 Viscous flux

The viscous flux is evaluated based on the cell-center gradients which have been computed for the inviscid flux, such that no further modifications at the flame front are necessary. The surface gradients are obtained with second-order accuracy by averaging the gradients on the adjacent cell centers.

4 Results

The presented method has been validated for a number of simple test cases, of which the merger of flame kernels is illustrated in Fig. 3 showing contours of the temperature, the velocity vectors, and iso-contours of the pressure as black lines. Solutions are shown for different time levels before and after the flame kernels coalesce. Initially, a quiescent flow field at ambient pressure with two circular flame kernels is prescribed. The flame Mach number is chosen as $M_f = 1 \times 10^{-3}$ corresponding to a laminar flame speed of approximately $s_l^u = 34cm/s$. Curvature corrections are not accounted for in this simulation, i.e., $s_\kappa^u = 0cm/s$. Due to this initialization, a pressure wave emanates from the flame front, which can be observed in Fig. 3a. A more detailed discussion of the test cases and the application of the presented method to large-eddy simulation of premixed combustion will be discussed at the conference.

Références

[1] Markstein G. Nonsteady flame propagation. Pergamon Press, 1964.

[2] Williams F. Turbulent Combustion. in : J.D. Buckmaster (Ed.), The mathematics of combustion, SIAM, 1985.

[3] Liou M.-S. and Steffen Jr. C. J. A new flux splitting scheme. J. Comput. Phys., 107, 23–39, 1993.

[4] Meinke M., Schröder W., Krause E., and Rister T. A comparison of second- and sixth-order methods for large-eddy simulation. Comput. Fluids, 31, 695–718, 2002.

[5] Fedkiw R., Aslam T., and Xu S. The ghost fluid method for deflagration and detonation discontinuities. J. Comput. Phys., 154, 393–427, 1999.

[6] Gómez P., Hernández J., and López J. On the reinitialization procedure in a narrow-band locally refined level set method for interfacial flows. Int. J. Numer. Meth. Engng, 63, 1478–1512, 2005.

[7] Herrmann M. A balanced force refined level set grid method for two-phase flows on unstructured flow solver grids. J. Comput. Phys., 227, 2674–2706, 2008.

[8] Hartmann D., Meinke M., and Schröder W. Differential equation based constrained reinitialization for level set methods. J. Comput. Phys., 227, 6821–6845, 2008.

[9] Sussman M., Smereka P., and Osher S. A level set approach for computing solutions to incompressible two-phase flow. J. Comput. Phys., 114, 146–159, 1994.

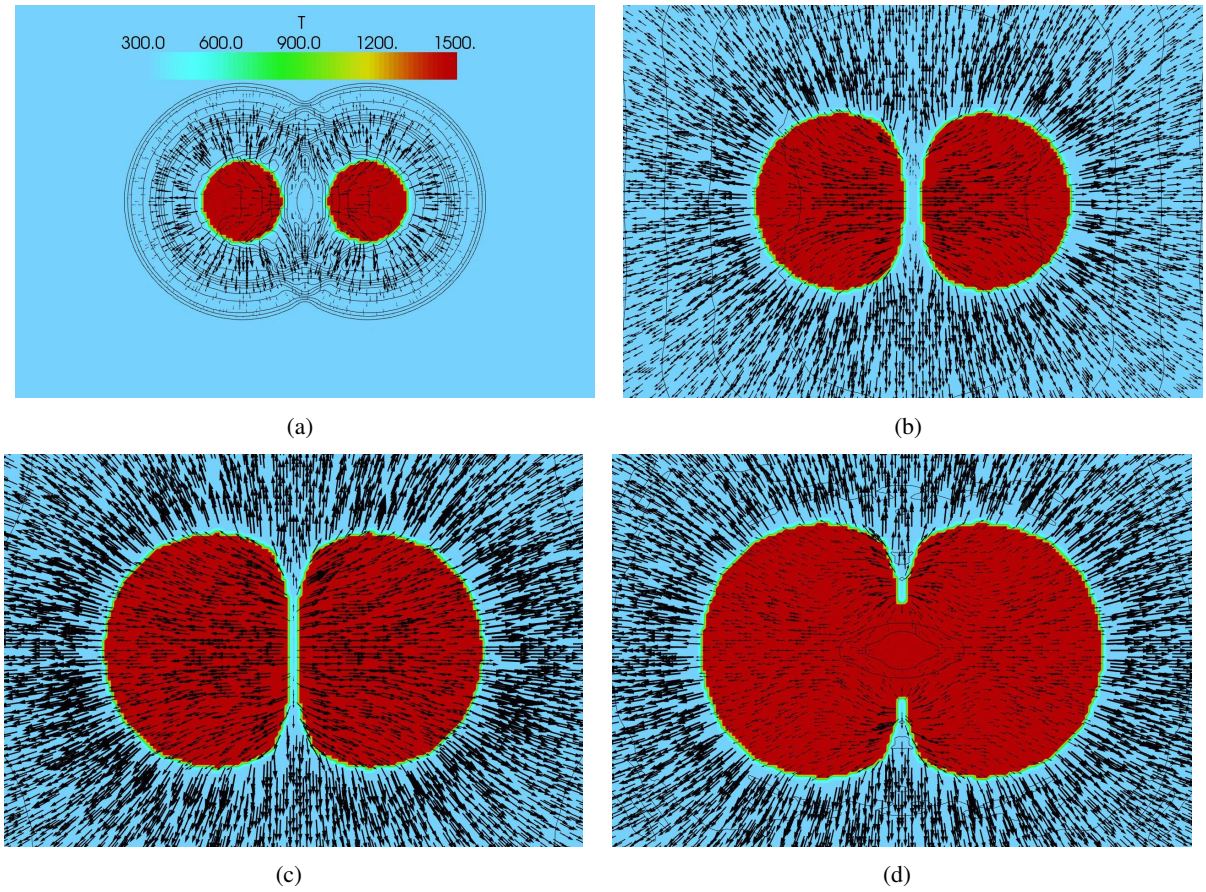

FIG. 3 – Fully compressible solution of coalescing flame kernels at different non-dimensional time levels : (a) $t = 1.75 \times 10^{-4}$; (b) $t = 1.12 \times 10^{-2}$; (c) $t = 1.75 \times 10^{-2}$; (d) $t = 2.0 \times 10^{-2}$. The temperature contours and the velocity vectors are shown. Black lines : pressure contours.

[10] Hartmann D., Meinke M., and Schröder W. On accuracy and efficiency of constrained reinitialization. Submitted to Int. J. Numer. Meth. Fluids, 2008.

[11] Hartmann D., Meinke M., and Schröder W. The constrained reinitialization equation for level set methods. Submitted to J. Comp. Phys., 2009.

[12] Peng D., Merriman B., Osher S., Zhao H., and Kang M. A PDE-based fast local level set method. J. Comput. Phys., 155, 410–438, 1999.

[13] Hartmann D., Meinke M., and Schröder W. An adaptive multilevel multigrid formulation for Cartesian hierarchical grid methods. Comput. Fluids, 37, 1103–1125, 2008.

[14] Hartmann D., Meinke M., and Schröder W. A general formulation of boundary conditions on Cartesian cut cells for compressible viscous flow. AIAA-Paper 2009-3878, 2009.

[15] van Leer B. Towards the ultimate conservative difference scheme. V. A second-order sequel to Godunov's method. J. Comput. Phys., 32, 101–136, 1979.